Thin Solid Films xxx (2011) xxx–xxx

Contents lists available at ScienceDirect

Thin Solid Films

journal homepage: www.elsevier.com/locate/tsf

Streak spectrograph temperature analysis from electrically exploded Ni/Al nanolaminates

Christopher J. Morris [a,*], Paul Wilkins [b], Chadd May [b], Eugene Zakar [a], Timothy P. Weihs [c]

[a] U.S. Army Research Laboratory, 2800 Powder Mill Rd, Adelphi, MD 20783, United States
[b] Lawrence Livermore National Laboratory, 7000 East Avenue, Livermore, CA 94550, United States
[c] Department of Materials Science and Engineering, The Johns Hopkins University, 3400 North Charles Street, Baltimore, MD 21218, United States

ARTICLE INFO

Available online xxxx

Keywords:
Exothermic mixing
Reactive laminates
Streak camera spectroscopy
Plasma temperatures

ABSTRACT

We report on electrically-induced heating and mixing of multilayered nickel/aluminum (Ni/Al) laminates observed by streak camera emission spectroscopy. Past experiments probing the kinetic energy of material ejected from the reaction zone indicate that additional kinetic energy originates from Ni/Al samples, presumably from exothermic mixing between the two metals. Here we examine streak spectrographs of similar experiments to determine the presence of expected elements and their temperatures. We conducted these experiments in rough vacuum, but found the emission to be dominated by argon (Ar) and nitrogen (N) lines in addition to the expected emission of Al and Ni, which were also present. Using the spectral information of Ar, we analyzed the relative intensities of four Ar peaks between 425 and 455 nm, with respect to their expected Boltzmann distributions to yield temperatures as a function of time. These temperatures were 2.24–2.59 eV for Al samples, and 2.93–3.27 eV for both Ni and Ni/Al samples, and were within estimates based on the measured electrical energy delivered to each device. The higher Ni/Al sample temperatures seemed to validate our past measurements of increased kinetic energy and the apparent rapid exothermic mixing between Ni and Al, although Ni samples yielded surprisingly high temperatures as well. These results may be important for future nanomanufacturing techniques involving localized heating from reactive Ni/Al multilayers, where the precise control of spatial temperatures may necessitate an equally precise temporal control of the reaction.

Published by Elsevier B.V.

1. Introduction

The nickel–aluminum (Ni/Al) intermetallic system is useful for a variety of reactive material applications [1], including the initiation of subsequent reactions, thermal batteries [2], and the localized heating required by many welding and joining applications [3–5]. Reaction characteristics are well studied at the normal self-heating rates of 10^3–10^6 K/s, where the lateral reaction propagation of the Ni/Al system is driven by heat diffusion along and between the reactive layers, leading to propagation rates as high as 10 m/s in the case of multilayered Ni/Al [1], or as high as 100 m/s for other reactive multilayered systems [6]. At these heating rates and for typical metallic or semiconducting material thermal diffusivities, the temperature rise extends roughly 10 μm into any surrounding material every microsecond. Future nanomanufacturing techniques may require more precise control of spatial temperature distributions, and one way to achieve this control is through more rapid heating rates.

We recently reported on experiments where we electrically heated microscale Ni/Al slabs at 10^{11}–10^{12} K/s [7]. In these experiments, electrical current passed through 175 μm square, 2.8 μm thick structures of multilayered Ni/Al, which were covered with a polymer "flyer" layer. The structures vaporized and rapidly accelerated the flyer layer to several km/s within 50 ns, through expansion of gaseous products. We found that Ni/Al conductor layers contributed between 1.13 kJ/g and 2.26 kJ/g of additional kinetic energy to flyer velocities as compared with conductors composed only of Cu, evaluated at the same instantaneous input electrical energy levels. The similarity between this additional kinetic energy and the 1.2 kJ/g available from exothermic mixing of Ni/Al [8] suggested that the expected mixing contributed directly to increased flyer velocity. We more recently compared Ni/Al flyer velocities to those from devices composed only of Al or Ni, and found similar results [9], with the kinetic energy from Ni/Al samples exceeding that of either Al or Ni. Thus, although the kinetics of Ni/Al lateral reaction propagation should be too slow to cover any significant distance in these timescales, the electrically forced heating of an entire multilayer slab appears to lead to a similar exothermic release.

* Corresponding author at: U.S. Army Research Laboratory, RDRL-SER-L, 2800 Powder Mill Rd, Adelphi, MD 20783, United States. Tel.: +1 301 394 0950; fax: +1 301 394 4562.
E-mail address: christopher.j.morris58.civ@mail.mil (C.J. Morris).

0040-6090/$ – see front matter. Published by Elsevier B.V.
doi:10.1016/j.tsf.2011.07.043

Report Documentation Page

Form Approved
OMB No. 0704-0188

1. REPORT DATE	2. REPORT TYPE	3. DATES COVERED
2011		**00-00-2011 to 00-00-2011**

4. TITLE AND SUBTITLE	5a. CONTRACT NUMBER
Streak Spectrograph Temperature Analysis From Electrically Exploded Ni/Al Nanolaminates	5b. GRANT NUMBER
	5c. PROGRAM ELEMENT NUMBER
6. AUTHOR(S)	5d. PROJECT NUMBER
	5e. TASK NUMBER
	5f. WORK UNIT NUMBER
7. PERFORMING ORGANIZATION NAME(S) AND ADDRESS(ES) **U.S. Army Research Laboratory,2800 Powder Mill Rd,Adelphi,MD,20783**	8. PERFORMING ORGANIZATION REPORT NUMBER
9. SPONSORING/MONITORING AGENCY NAME(S) AND ADDRESS(ES)	10. SPONSOR/MONITOR'S ACRONYM(S)
	11. SPONSOR/MONITOR'S REPORT NUMBER(S)

12. DISTRIBUTION/AVAILABILITY STATEMENT
Approved for public release; distribution unlimited

13. SUPPLEMENTARY NOTES
Thin Solid Films (2011), Preprint, 6 pages

14. ABSTRACT

15. SUBJECT TERMS

16. SECURITY CLASSIFICATION OF:			17. LIMITATION OF ABSTRACT	18. NUMBER OF PAGES	19a. NAME OF RESPONSIBLE PERSON
a. REPORT	b. ABSTRACT	c. THIS PAGE			
unclassified	**unclassified**	**unclassified**	**Same as Report (SAR)**	**7**	

Here we report on electrically forced heating of Ni/Al as observed by streak camera emission spectroscopy. These experiments were performed with non-reactive Ni, Al, and multilayered reactive Ni/Al samples, each without the polymer flyer layer used in previously cited results. Without the flyer layer, and despite the fact that experiments were performed under vacuum, emission was dominated by residual argon (Ar) and nitrogen (N). Thus, the emission was stimulated by electrical arcing through both locally vaporized metal and residual gasses. Still, the relative intensities of Ar peaks and their expected Boltzmann distribution functions yielded temperature values for each sample as a function of time. The following section describes our fabrication, experimental, and temperature analysis methods in detail.

2. Methods

We fabricated devices as depicted in Fig. 1a, with the conductor layer formed of Ni, Al, or multilayered Ni/Al. The substrate in each case was quartz. For the Al samples, we sputtered 20 nm of titanium (Ti) followed by 2.7 μm of Al. The Ni samples contained a single 2.7 μm layer of sputtered Ni/V (93 wt.% Ni, 7 wt.% V). The Ni/Al samples contained a 20 nm Ti adhesion layer, and five iterations of sputtered Ni/V (200 nm) followed by Al (~300 nm), finishing with a sixth layer of Ni/V (~200 nm). The total Ni/Al stack was 2.64 μm in thickness. Sputtering power was approximately 6.6 and 3.1 W/cm^2 for Ni/V and Al, respectively. The base pressure prior to sputtering was less than 1×10^{-6} Torr, and the sputter gas was Ar at approximately 15 mTorr.

We performed lithographic patterning using a 2-μm-thick positive photoresist layer to define the 175 μm square bridge regions, shown in Fig. 1b. A wet etch removed all exposed conductor layers except Ti (Aluminum Etchant Type A, Transene Company, Inc., Danvers, Massachusetts). An HF solution diluted 50:1 with deionized water etched the remaining Ti for those sample types containing this layer. Finally, a resist stripper removed the photoresist (PRS-3000, JT Baker Inc., Phillipsburg, New Jersey), while kapton tape masked individual device contact pads. We diced the wafers into individual samples and removed the kapton tape masking to expose device contacts.

The experiment involved a series circuit consisting of a bridge wire device, a 0.12 μF capacitor charged to 1200 V, a switch, a 5 mΩ current viewing resistor (2 ns rise time), and low inductance strip line connecting all components. Without the bridge wire device, the response of current i in the circuit was

$$\frac{d^2i}{dt^2} + \frac{R}{L}\frac{di}{dt} + \frac{1}{LC}i = 0 \tag{1}$$

where L and R represent the total series inductance and resistance, respectively. By fitting the response of the circuit to the solution of Eq. (1), we determined inductance and resistance values of 3.7 nH and 38 mΩ, respectively, corresponding to an undamped natural frequency of 7.6 MHz. With added damping from the insertion of a bridge wire device into the circuit, the high voltage capacitive discharge resulted in a current pulse corresponding to a half cycle at 2.35 ±0.02 MHz, calculated from pulse widths averaging 213 ns. At this characteristic frequency, calculated skin depths were more than 40 times the thicknesses of conductors used in this study, so we assumed skin effects to be negligible.

We expected bridge resistance to be a strong function of instantaneous temperature induced by electrical current, so we monitored voltage drop using probes soldered to strip lines near the point of connection to each device. In general, the measured voltage drop V_m would be a combination of actual bridge voltage drop V_b and an impedance term resulting from any inductance in the bridge L_b,

$$V_m = V_b + L_b\frac{di}{dt} \tag{2}$$

This impedance term would cause the measured voltage to artificially increase at the onset of current rise and then level off, leading to a calculated bridge resistance that would start artificially high and then decrease with rising current. Because we only observed resistances which steadily increased from the start of each current pulse, as expected from temperature rise induced by increasing current, we assumed negligible bridge inductance such that $V_m = V_b$.

The streak spectrograph setup is shown in Fig. 2, where a plexiglass vacuum chamber held the sample and provided connections to the firing circuit described above. The chamber was pumped to approximately 10 mTorr before each test. An 85 mm, f1.4 lens focused the light into a 400 μm diameter optical fiber, and another 105 mm f1.8 lens collimated the light towards a 1200 mm^{-1} grating. A second 105 mm f1.8 lens focused the light into a streak camera (EG&G model L-CA-24) which was connected to a 16-bit monochrome, 4096×4096 pixel CCD camera (Spectral Instruments, 800-175).

Using the 1200 mm^{-1} grating, we captured several streak images from 405, 532, and 655 nm laser sources, a comb generator, and a mercury arc lamp, all of which allowed us to calibrate the output of the grating and temporal resolution of the streak camera, estimate the optical resolution, and correct for some optical path inefficiencies. The usable wavelength range was approximately 140 nm at 22.05 pixels/nm, and the temporal range was 350 ns at 10.74 pixels/ns. By centering the grating at 450 nm and 532 nm over two separate experiments, we could span the wavelength range of 380 nm to 600 nm. Based on a Gaussian fit to several laser lines, we estimated the optical resolution of this setup to be 2.0 nm. Finally, although we did not have ready access to a calibrated background light source to correct for differences in detector sensitivity to different wavelengths,

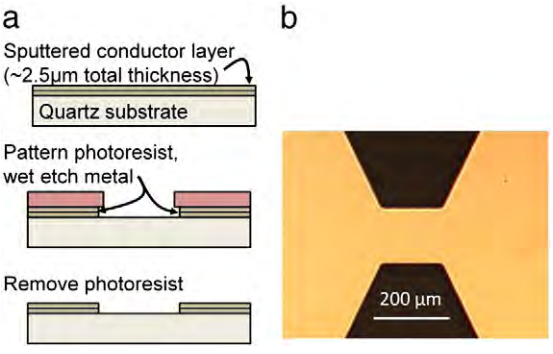

Fig. 1. Fabrication process flow and microscope image of completed device.

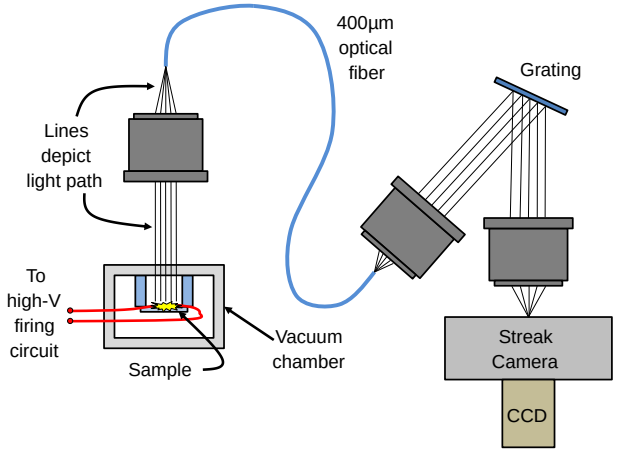

Fig. 2. Streak spectrograph test setup. Vacuum chamber was pumped to approximately 10 mTorr.

Please cite this article as: C.J. Morris, et al., Thin Solid Films (2011), doi:10.1016/j.tsf.2011.07.043

we did subtract a dark current background from each image which accounted for about 0.2% of each image pixel's dynamic range. We also corrected for optical path inefficiencies along the time axis using a radial dual-Gaussian correction function that forced streak images from continuous laser sources to be constant over time. We then performed this same correction to all subsequent captured streak images.

In addition to the data gathered with the 1200 mm^{-1} grating, we acquired a partial set of data using a 600 mm^{-1} grating, centered at 532 nm. This setup allowed a wavelength range with each experiment of approximately 380 to 680 nm, with an optical resolution of 3.1 nm.

To investigate the apparent temperature values associated with bridge bursts, we compared the relative intensities of various peaks, each at wavelength λ, with the expected Boltzmann distribution equation. This equation yields a linear relationship between the logarithm of the peak intensity I and the energy E_i of the excited state associated with the peak [10],

$$ln\left(\frac{I\lambda}{g_k A_{ki}}\right) = -\frac{E_i}{kT} + C \tag{3}$$

In Eq. (3), g_k is the partition coefficient associated with the excited level, A_{ki} is the transition probability, the non-subscript k is Boltzmann's constant, and C is a constant associated with the ground state. The slope of this linear relationship is equal to $-1/kT$. This method relies on the assumption that emission intensities are not affected by self-absorption, which may or may not apply during the early stages of a rapidly expanding cloud of vaporized material. The method also relies on intensities being proportional to actual line radiance, and therefore generally requires detector calibration across the range of wavelengths used.

We selected four Ar lines shown in Table 1 for the Boltzmann plots, representing a 30 nm wavelength range near the center of each spectrum. We considered this range to be sufficiently small to waive the requirement for detector calibration across all wavelengths. The partition and transition parameters in Table 1 are from [11], and energy values are from [12]. Using these values and intensities from digitized streak images, we used Eq. (3) to calculate the slope from a least squares linear fit, from which we calculated temperature as a function of time for each sample type.

If we were to iteratively correct the intensity of each peak for blackbody emission at the calculated temperature, the actual emission intensity at 425 nm would be 79% of that at 455 nm, according to Plank's equation evaluated at a temperature of 3 eV. Eq. (3) shows that a factor of 0.79 on intensity would result in a −0.23 offset on calculated vertical axis values, which we found to affect calculated temperatures by a maximum of 3.9%. In related work investigating the emission of laser ablated Al/Teflon films, time-resolved through the use of a streak camera, the observed broadband emission was not attributed to classical blackbody radiation, because it did not change with increasing laser irradiance as would be expected [13]. Therefore, we did not attribute our emission to that of a classical blackbody source, and did not perform corrections based on Plank's equation.

Table 1
Spectroscopic parameters of Ar lines.

Spectrum	Wavelength (nm)	Energy of upper level (eV)	$g_k A_{ki}$ (10^8 s^{-1})
Ar-II	427.8	21.35	0.320
Ar-II	433.1	19.61	2.30
Ar-I	451.1	3.028	0.0118
Ar-II	454.5	19.87	1.884

3. Results and discussion

3.1. Spectroscopic results

Fig. 3 shows a typical streak spectrograph, obtained from a Ni/Al laminate using the 600 mm^{-1} grating. The initial time of zero was defined as the point at which the average intensity across all wavelengths was half its maximum, therefore corresponding closely to the time of burst and maximum intensity. Similar to related studies of other energetic materials over longer timescales [14], a typical captured image featured an initial period of nearly broadband emission, with superimposed spectral peaks which quickly grew in intensity. Such broadband emission has been observed for other reactive, Al-based nanothermite materials [15], as well as with laser ablation of Al/Teflon films [13]. The multilayered Ni/Al samples generally exhibited an overall brightness that was higher and persisted longer than either Al or Ni samples.

Figs. 4, 5, and 6 show streak spectrographs of Al, Ni, and Al–Ni bridges at 10, 50, and 250 ns following the onset of emission, or burst, utilizing the 1200 mm^{-1} grating. Although performed under vacuum, the similar emission in each case suggests elements from residual gasses in the vacuum chamber. We attributed many of the common peaks to Ar and nitrogen (N), which likely came from the surrounding atmosphere at 10 mTorr, a common pressure range at which Ar plasmas are used in microfabrication processes [16]. Given that Ar was used during the sputter deposition process, it was also possible for Ar to originate from the films themselves, which for Ni films at the sputtering conditions used can be on the order of 0.3% by atomic ratio [17].

Emission peaks indicating Al and possibly Ni were also present. Specifically, Fig. 4 shows the prominent doublet at 394.4/396.1 nm indicating vapor phase atomic Al, which was not present in the Ni samples as expected. Also labeled are Ar-I and Ar-II lines at 407.2, 413.2, 415.9, 420.1, 427.8 and 433.1 nm. The broad doublet near 450 nm was actually a combination of several possible lines: N-II at 444.7 nm, Ni-I at 447.0 nm (for Ni and Ni/Al samples only), Ar-I at 447.5 and 451.1 nm, Ar-II at 448.2 nm, and N-III at 451.1 nm. The cluster of peaks just past 460 nm was likely from Ar-II at 459 and 461, and at least five N-I and N-IV peaks were between 460.1 and 462.4 nm. Lastly, Ar-II at 498 nm is also labeled. Fig. 5 shows the same lines at 50 ns following the onset of emission. Some lines became more prominent including a clear shift in the Al sample line near 460 nm, which we have labeled Al-II at 466.7 nm. Fig. 6 at 250 ns following the onset of emission shows the best evidence of residual gas signatures, where many of the Ni sample lines clearly coincided with Al sample lines. The boxed labels in Fig. 6 indicate the four Ar lines

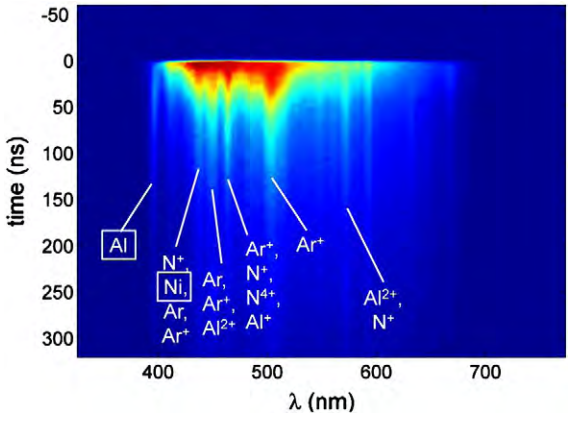

Fig. 3. Streak spectrograph of a Ni/Al bridge fired at 1.2 kV, viewed with a 600 mm^{-1} grating.

Please cite this article as: C.J. Morris, et al., Thin Solid Films (2011), doi:10.1016/j.tsf.2011.07.043

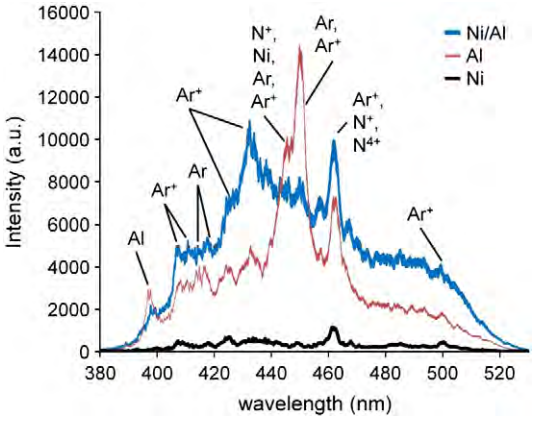

Fig. 4. Ni/Al, Al, and Ni sample emission at 10 ns following the onset of emission, over wavelengths of 380 to 520 nm, with major peaks identified.

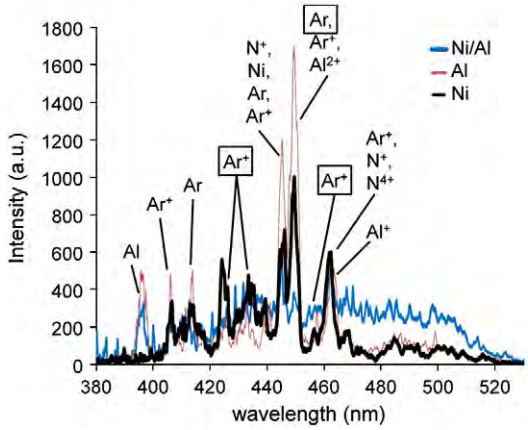

Fig. 6. Ni/Al, Al, and Ni sample emission at 250 ns following the onset of emission, over wavelengths of 380 to 520 nm, with major peaks identified. The three boxed labels refer to the four Ar lines used for temperature analysis by comparison to intensities predicted by the Boltzmann equation.

that are listed in Table 1 and are used for temperature analysis in the following section.

Fig. 7 shows emission at 100 ns following the onset of emission in the wavelength range of 450 nm to 610 nm. While many of the lines in Figs. 4–6 were attributed to Ar, Fig. 7 provides clear evidence that nitrogen emission was also present, because the prominent, common peaks near 570 nm coincided best with N-II lines at 566.7, 567.6, 568, 568.6, and 571.1 nm. Therefore, although some Ar could have originated from the common deposition process used to deposit the films, residual gasses in the test chamber were the most likely source for the observed N emission. Lines from Al-III at 569.6 and 572.3 nm were also present in the Al sample in Fig. 7, but less so in the Ni/Al sample. Fig. 7 also provides evidence of vapor phase Ni-I at 508.1 nm, present in both the Ni and Ni/Al sample traces.

Although several lines were observed between 450 and 550 nm, we did not attribute them to aluminum oxide, which normally occurs in processes involving highly-reactive Al and any presence of atmospheric oxygen [14,18,19]. The fact that any lines in this wavelength range were also present in the emission from Ni samples indicates that our timescales were not long enough to allow convective mixing between Al and atmospheric oxygen. Due to the multilayered nature of the Ni/Al samples, however, very little convection would be required for exothermic mixing to occur.

3.2. Temperature analysis

To calculate temperatures, Fig. 8 shows a typical linear fit of four Ar line intensities and spectroscopic parameters from Table 1, plotted according to Eq. (1). This particular plot is from a Ni/Al sample at 100 ns following burst. The R-squared value was 0.998, and the slope corresponded to a temperature of 3.07 eV, or 35,650 K. In general, the linear fit quality was quite high, with R-squared values ranging from 0.964 to 0.999. Although there were at least sixteen other significant Ar peaks between 425 and 465 nm, all except three of the four Ar lines specified were too close in wavelength to significant Al, Ni, and N lines, and our experimental setup could not resolve them. One of the four lines used, 451.1 nm, may also have been coincident with a moderately significant line from doubly ionized nitrogen. However, we used this line with spectroscopic parameters from Ar in order to include enough energy level variation to yield reasonable approximations of slope and therefore temperature. Recognizing that the intensity of this particular line may have been influenced by N emission, Fig. 8 shows that even a factor of two in intensity difference at the 3 eV level would only lead to a difference in slope of approximately 12%. Therefore, we safely assumed that the intensity of this line was primarily from Ar emission.

Fig. 9 shows temperature as a function of time predicted by the Boltzmann equation for Al, Ni, and multilayered Ni/Al samples, with data from two samples of each type in order to show typical variation from sample to sample. The temperatures were quite high, with all samples starting at 3.1–3.4 eV, and then either rising or falling to relatively constant values after 150 ns. The final temperatures at 300 ns were 2.30–2.54 eV (26,700 to 29,500 K) for Al, and 3.19–3.33 eV for both Ni/Al and surprisingly, Ni. Fig. 10 also shows temperatures calculated from experiments using the 600 mm^{-1} grating, where the averaging effect of lower optical resolution led to

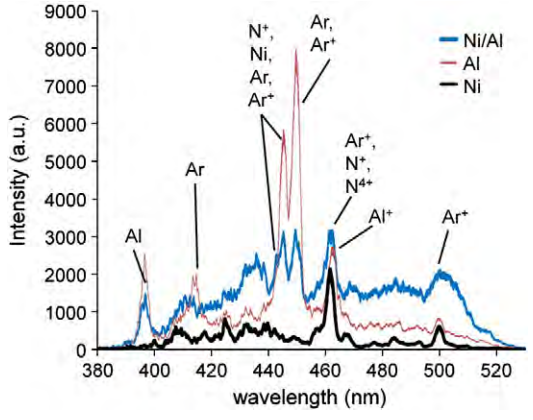

Fig. 5. Ni/Al, Al, and Ni sample emission at 50 ns following the onset of emission, over wavelengths of 380 to 520 nm, with major peaks identified.

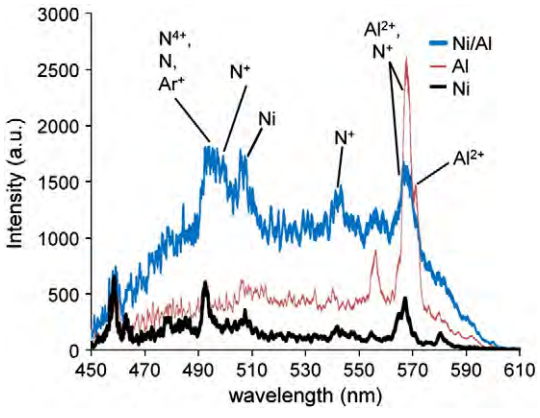

Fig. 7. Ni/Al, Al, and Ni sample emission at 100 ns following the onset of emission, over wavelengths of 450 to 610 nm, with major peaks identified.

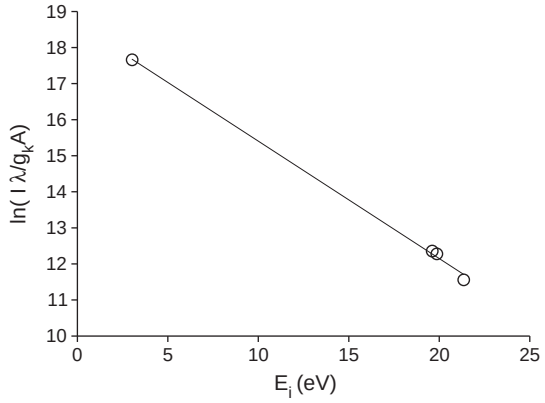

Fig. 8. Linear fit to a plot of four Ar line intensities and spectroscopic parameters in Table 1 vs energy according to Eq. (1), for a Ni/Al sample at 100 ns following the onset of emission. The R-squared value was 0.998, and the slope corresponded to a temperature of 35,650 K, or 3.07 eV.

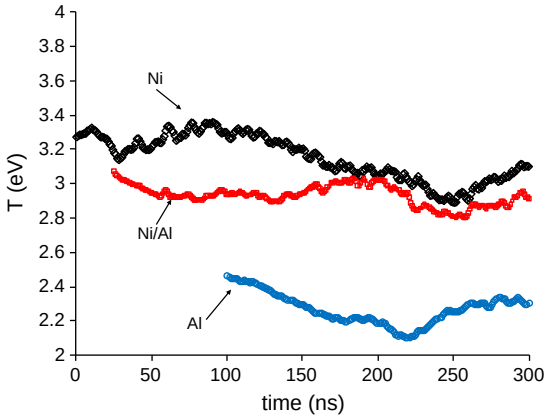

Fig. 10. Temperature vs time predicted by the Boltzmann equation for one sample each of Al, Ni, and multilayered Ni/Al, each obtained with a 600 mm^{-1} grating. The intensities of several lines from both the Al and Ni/Al samples were unavailable at early times due to detector saturation, so data covering these time intervals are not shown.

less scatter in the data and yielded temperatures generally within 0.3 eV of the calculations using the 1200 mm^{-1} grating. The intensity of emission was approximately four times brighter than with the 1200 mm^{-1} grating, so the similar temperature calculations indicate that any non-linearity in detector response at higher signals was consistent over the wavelengths studied. As indicated in the caption, the higher intensities of several lines from both Al and Ni/Al samples saturated the detector at early times.

Other lines from which we could have calculated temperatures include those from N, Ni, or Al. However, the prominent N lines covered too narrow an energy range to yield good slope approximations. Similarly, the few Ni lines annotated in the figures were very close in energy levels, and except for the Ni line annotated in Fig. 7, they were not distinct from other Ar and N lines. There were several Al lines, but the only distinct ones were at 394.4 and 396.2 nm, which are at nearly identical energy levels. Using four other Al lines at 452.9, 466.7, 569.7, and 572.2 nm, which span energy levels between 13 and 20 eV, a linear fit for Al at 250 ns yielded an R-squared value of 0.41 and a temperature of 2.56 eV. This temperature was close to the temperatures shown in Figs. 9 and 10 at 250 ns, and although this level of similarity was not observed for all Al samples at all times, the fact that similar temperatures were obtained using measurements and parameters for a different element suggests that temperatures obtained through analysis of Ar spectral lines were accurate.

We also calculated energy input to each sample by integrating the product of measured current and voltage through each bridge. Fig. 11 shows the cumulative energy through each of the three samples which produced the streak spectrographs in Figs. 4–6. The point of maximum resistance for each sample occurred at $t=0$, corresponding with the point of maximum voltage and bridge burst [20], and therefore corresponding closely with $t=0$ in the spectroscopic and temperature plots. Assuming all energy went into heating the bridges defined by their original dimensions, 2.78 mJ, 5.57 mJ, and 4.02 mJ were required to atomize (i.e., heat, melt, and vaporize) the Al, Ni, and Ni/Al samples, respectively. As indicated by the inset of Fig. 11, the Al and Ni/Al samples were likely atomized at $t=0$, and the Ni sample reached its atomization energy at 12.2 ns.

The cumulative energies into each sample were enough to fully ionize and generate the temperatures observed. The energy into the Al sample was enough to ionize it by 14.5 ns, and the presence of ionized Al agrees qualitatively with Figs. 4 and 5 showing the Al-II peak at 466.7 nm, present at 50 ns but not at 10 ns. The energy into the Al sample was also sufficient to doubly ionize it at 71 ns. Fig. 6 shows an Al-III peak at 453 nm, while Fig. 7 shows Al-III at 569.6 and 572.3 nm. By 300 ns, approximately 72% of the Al sample could be triply ionized with 2.4 eV/atom remaining to contribute to the temperature of 2.4 eV calculated in Figs. 9 and 10. The Ni sample reached its first ionization level at 50 ns, and by 300 ns, 76% of the sample could be doubly ionized with 3.4 eV/atom remaining to correspond to calculated temperatures at that time. Finally, the Ni/Al sample reached the first ionization energy of its Al and Ni components at 8.3 ns and 23 ns, respectively, and the second ionization energy of its

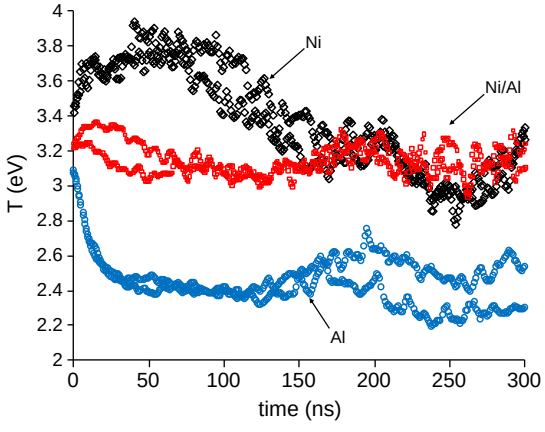

Fig. 9. Temperature vs time predicted by the Boltzmann equation for two samples each of Al, Ni, and multilayered Ni/Al, each obtained with a 1200 mm^{-1} grating.

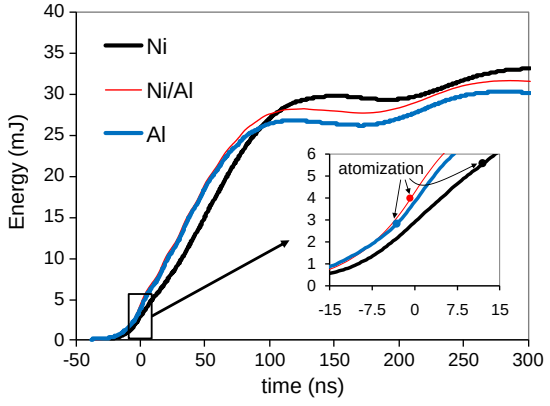

Fig. 11. Electrical energy dissipated vs time in Al, Ni, and Ni/Al bridges, calculated from integration of current and voltage measurements through each sample. Inset shows detail of energies dissipated at $t=0$, corresponding closely to theoretical energies required for atomization of each sample type.

Al component by 52.3 ns. By 300 ns, 85% of the remaining Ni component could be doubly ionized leaving 3.0 eV/atom to correspond to calculated temperatures at that time. Of course, the prediction of how energy distributed between temperature and ionized specie proportions is not necessarily valid, but we present these values to demonstrate that sufficient energy was supplied to each sample to generate the species observed and temperatures calculated. Plasma temperatures in the range of 1 eV up to several hundred eV are commonly calculated from electrically exploding wires and other short duration plasma discharges [21–24].

The higher temperatures of Ni/Al compared with Al may provide evidence of additional energy from exothermic mixing of Ni/Al. However, calculated Ni temperatures were actually higher than those of multilayered Ni/Al at early times, and cooled to similar levels at later times. This result was surprising given that the overall emission of Ni samples was lower than either of the Al or Ni/Al samples, but given the consistently high correlation of linear fits to the Boltzman equation, the calculated effective temperatures appear to be accurate. It is possible that the higher calculated temperature was simply that of surrounding Ar plasma, and not the Ni itself, perhaps due to higher Ni resistivity causing more current to flow through the surrounding ionized atmosphere.

Regardless of temperature, the presence of atomic Al and Ni spectral lines indicate that atomic species of these elements were present. Although there was also evidence of singly and doubly ionized Al, there were significant levels of Al atoms excited from their ground state, suggesting that they were available to exothermically mix with Ni. To better show evidence of exothermic behavior between Ni and Al under these conditions, we plan future tests with samples covered by a flyer layer as in [7]. We expect this layer to limit the stimulation of Ar and N emission, and enhance emission from vaporized conductor materials. Although it is possible that varying amounts of Ar may be trapped in the films from the sputter deposition process, temperature estimates would better represent the films themselves instead of any surrounding atmosphere. Also, better calibration of the detector would allow quantification over a wider wavelength range, as well as allow temperature determination through alternative methods such as pyrometry. We hope to carry out these tests in the near future, but the present set of results suggests that exothermic mixing of Ni/Al is possible from rapidly heated and vaporized material.

4. Conclusions

The goal of this study was to validate past results suggesting that Ni/Al exothermic mixing can be electrically forced to occur over very short timescales. Time resolved streak spectroscopy of multilayered and single component bridges indicated that emission from multilayered Ni/Al samples exhibited an overall brightness that was higher and persisted longer than either Al or Ni control samples. The atomic Al and Ni spectral lines in these experiments indicate that atomic species of these elements were present, along with weaker lines indicating ionic species. We calculated temperatures to be in the range of 3.1–3.4 eV within the first few nanoseconds of the onset of emission, with Al samples cooling to roughly 2.46 eV after 300 ns, and Ni/Al samples remaining around 3.27 eV. Nickel samples yielded temperatures which first increased, then decreased to the same level as those of Ni/Al samples. Although these temperature levels were high, they were reasonable for localized plasma temperatures given the level of electrical energy supplied to each device.

Further testing should aim to limit the interaction of metallic sample emission and electrical arcing through residual atmospheric elements. Doing so will better isolate individual Al and Ni spectral lines, and insure that temperatures better reflect the rapidly heated metallic species. Still, results reported here support the hypothesis that Ni/Al exothermic mixing is possible from material which is electrically heated at extremely short timescales.

Acknowledgements

The authors gratefully acknowledge Dr. Kevin McNesby at U.S. Army Research Laboratory for helpful discussions on analysis of streak emission spectroscopy. Professor T.P. Weihs acknowledges the financial support of the Office Naval Research through Grant No. N00014-07-1-0740.

References

[1] A.J. Gavens, D.V. Heerden, A.B. Mann, M.E. Reiss, T.P. Weihs, J. Appl. Phys. 87 (2000) 1255.
[2] M. Ding, F. Krieger, J. Swank, C. McMullan, G. Chen, J. Poret (Eds.), 2008 NDIA Power & Energy Workshop, Warren, MI, 2008.
[3] A.J. Swiston, T.C. Hufnagel, T.P. Weihs, Scr. Mater. 48 (2003) 1575.
[4] J. Wang, E. Besnoin, A. Duckham, S.J. Spey, M.E. Reiss, O.M. Knio, M. Powers, M. Whitener, T.P. Weihs, Appl. Phys. Lett. 83 (2003) 3987.
[5] B. Boettge, J. Braeuer, M. Wiemer, M. Petzold, J. Bagdahn, T. Gessner, J. Micromech. Microeng. 20 (2010) 064018.
[6] A.S. Rogachev, Russ. Chem. Rev. 77 (2008) 21.
[7] C.J. Morris, B. Mary, E. Zakar, S. Barron, G. Fritz, O. Knio, T.P. Weihs, R. Hodgin, P. Wilkins, C. May, J. Phys. Chem. Solids 71 (2010) 84.
[8] V.M. Sandakov, Y.O. Esin, P.V. Gel'd, Russ. J. Phys. Chem. 1020 (1971) 45.
[9] C.J. Morris, P. Zakar, Eugene Wilkins, C. May, T.P. Weihs, in Proc. 27th Annual Army Science Conference, Orlando, FL.
[10] I. Reif, V.A. Fassel, R.N. Kniseley, Spectrochim. Acta, Part B 28 (1973) 105.
[11] J.R. Fuhr, W.L. Wiese, L.I. Podobedova, D.E. Kelleher (Eds.), CRC Handbook of Chemistry and Physics, 91st edition, CRC Press, 2010.
[12] G. Norlén, Phys. Scr. 8 (1973) 249.
[13] R.W. Conner, D.D. Dlott, J. Phys. Chem. A 114 (2010) 6731.
[14] J.R. Carney, J.S. Miller, J.C. Gump, G.I. Pangilinan, Rev. Sci. Instrum. 77 (2006) 063103.
[15] D.S. Moore, S. Son, B. Asay, Propellants Explos. Pyrotech. 29 (2004) 106.
[16] D. Boonyawan, S. Davydov, B. Yotsombat, N. Chirapatpimol, T. Vilaithong, Rev. Sci. Instrum. 73 (2002) 754.
[17] H.F. Winters, E. Kay, J. Appl. Phys. 38 (1967) 3928.
[18] P. Lynch, H. Krier, N. Glumac, J. Thermophys Heat Transfer 24 (2010) 301.
[19] N. Glumac, H. Krier, T. Bazyn, R. Eyer, Combust. Sci. Technol. 177 (2005) 485.
[20] R. Baksht, A. Pokryvailo, Y. Yankelevich, I. Ziv, J. Appl. Phys. 96 (2004) 6061.
[21] P.G. Burkhalter, C.M. Dozier, D.J. Nagel, Phys. Rev. A 15 (1977) 700.
[22] A.Y. Faenov, S.Y. Khakhalin, A.A. Kolomensky, S.A. Pikuz, A.I. Samokhin, I.Y. Skobelev, J. Phys. D: Appl. Phys. 18 (1985) 1347.
[23] X. Zhou, Y. Li, J. Wang, Z. Huang, IEEE Trans. Plasma Sci. 29 (2001) 360.
[24] G.S. Sarkisov, S.E. Rosenthal, K.R. Cochrane, K.W. Struve, C. Deeney, D.H. McDaniel, Phys. Rev. E 71 (2005) 046404.

Please cite this article as: C.J. Morris, et al., Thin Solid Films (2011), doi:10.1016/j.tsf.2011.07.043